






## RESEARCH LETTER

10.1029/2023GL103297

# Decoupled Indian Summer Monsoon Intensity and Effective Moisture Since the Last Glaciation in Southwest China

Tingwei Zhang<sup>1</sup> , Xiaoqiang Yang<sup>1</sup> , Jie Peng<sup>1</sup>, Qixian Zhou<sup>1</sup>, Jaime Toney<sup>2</sup> , Huiyang Liu<sup>1</sup>, and Yixuan Xie<sup>1</sup>

<sup>1</sup>School of Earth Science and Engineering, Guangdong Provincial Key Laboratory of Geodynamics and Geohazards, Southern Marine Science and Engineering Guangdong Laboratory (Zhuhai), Sun Yat-sen University, Guangzhou, China, <sup>2</sup>School of Geographical and Earth Sciences, University of Glasgow, Glasgow, UK

### Key Points:

- The long-term effective moisture (EM) record in Southwest China since ~90 kyr was reconstructed
- The EM variability at the orbital scale in terrestrial Indian summer monsoon region is primarily dominated by precession
- The topographic barrier and temperature induced aridification contribute to the decoupling of monsoon intensity and EM

### Supporting Information:

Supporting Information may be found in the online version of this article.

### Correspondence to:

X. Yang,  
eesyxq@mail.sysu.edu.cn

### Citation:

Zhang, T., Yang, X., Peng, J., Zhou, Q., Toney, J., Liu, H., & Xie, Y. (2023). Decoupled Indian summer monsoon intensity and effective moisture since the last glaciation in Southwest China. *Geophysical Research Letters*, 50, e2023GL103297. <https://doi.org/10.1029/2023GL103297>

Received 17 FEB 2023  
Accepted 12 MAY 2023

### Author Contributions:

**Data curation:** Tingwei Zhang, Jie Peng, Qixian Zhou, Jaime Toney, Huiyang Liu, Yixuan Xie

**Formal analysis:** Tingwei Zhang  
**Investigation:** Tingwei Zhang, Xiaoqiang Yang, Jie Peng, Qixian Zhou, Jaime Toney, Huiyang Liu, Yixuan Xie

**Methodology:** Tingwei Zhang

**Project Administration:** Xiaoqiang Yang

**Supervision:** Xiaoqiang Yang

**Visualization:** Tingwei Zhang

**Writing – original draft:** Tingwei Zhang, Xiaoqiang Yang

**Abstract** Effective moisture (EM) distribution in the Indian summer monsoon (ISM) region is strongly related to regional topography. An understanding of climate change and the interactions between climate variables can help predict future climate variations. Here, we reconstruct a stack EM record for Southwest China over the past 90 kyr using environmental magnetism in lake sediment. The EM in Southwest China at the orbital scale was closely linked to precession-induced change in North Hemisphere solar insolation, as well as the ISM variability. However, at the glacial-interglacial scale, it was decoupled with ISM intensity, being wetter during glacial periods (weakened ISM) and drier during interglacial periods (enhanced ISM). Combined with modern meteorological observations, we suggest that the topographical barrier effect and temperature induced dryness are responsible for the decoupling between ISM intensity and EM. The terrestrial topography and temperature strongly influence EM distribution by altering the dynamics of onshore airflow and evapotranspiration.

**Plain Language Summary** Effective moisture (EM) directly affects hydrological cycle and wider-scale socio-economic development. Reconstruction of prehistoric EM levels is essential for deeper understanding of the global climate system, developing climate models and improving prediction of future climate variations. Here, we reconstruct a high-resolution EM record over the past ~90,000 years from lake sediments in Tengchong, Yunnan province, Southwest China. We found that the variation of precession (shifts in the rotational axis of the Earth) and solar insolation are the key contributors to the EM variability at the orbital scale. Unusually, a wetter climate during the glacial period and relatively drier interglacial periods were observed in our records, which is opposite to those found in previous studies (arid glacial and humid interglacial) in monsoon regions, indicating a decoupling pattern between monsoon intensity and EM in study region. Based on a comprehensive analysis of the modern meteorological observations, we conclude that the topography and temperature exert a considerable role in modulating EM distribution and response to the decoupling pattern.

## 1. Introduction

The Indian summer monsoon (ISM), a critical component of the Asian monsoon system, transports massive amounts of heat and moisture from the Indian Ocean to the Indian subcontinent and inland China (An et al., 2011). Variations in the monsoon system directly affect the livelihood of billions of people and the wider socio-economic development in these regions (Jin & Wang, 2017; S. Li et al., 2018; X. Li & Tang, 2021). Changes in paleo-monsoonal precipitation and its influencing factors have long been a matter of great concern for assessing climatic variability and predicting future climatic changes. To date, substantial progress has been made in reconstructing monsoon variability since the Pleistocene (e.g., Cai et al., 2015; Cheng et al., 2016; Kathayat et al., 2016; Kathayat et al., 2022). It is now widely believed that precipitation decreased during the last glacial period (LGP) in Southwest China, which is attributed to a diminution of the ISM (Tian et al., 2019; Zhao et al., 2021). However, the ISM moisture transmission involves multiple interactions of the large-scale atmosphere-oceans circulation and the more localized topography (Acosta & Huber, 2020; Cai et al., 2015; Ding et al., 2020; Man et al., 2014; R. Zhang et al., 2015; Zhou et al., 2010). The topographic barrier may modulate the monsoon circulation and redistribute water vapor (Acosta & Huber, 2020; Xie et al., 2006; R. Zhang et al., 2015). Moreover, climatic records in Southwest China are mostly distributed on the eastern side of the mountains, and previous high-resolution last glacial records with respect to ISM precipitation variation in Southwest China are

© 2023. The Authors.

This is an open access article under the terms of the [Creative Commons Attribution License](https://creativecommons.org/licenses/by/4.0/), which permits use, distribution and reproduction in any medium, provided the original work is properly cited.

limited to speleothem stable oxygen isotope ( $\delta^{18}\text{O}$ ) records (e.g., Cai et al., 2015; Cheng et al., 2016). Effective moisture (EM), which is calculated from precipitation and evapotranspiration, is more effective than precipitation at describing whether a region is wetter or drier as it takes the water demand into account (S. Liu et al., 2018). Hence, reconstructions of the EM variation along the windward slopes of mountains in Southwest China over the LGP are needed to decipher the precipitation and EM pattern and to accurately evaluate the forcing mechanism.

Tenchong Qinghai (TCQH) Lake ( $25^{\circ}07'48''\text{N}$ – $25^{\circ}08'6''\text{N}$ ,  $98^{\circ}34'11''\text{E}$ – $98^{\circ}34'16''\text{E}$ ) is situated in the western Gaoligong Mountains (GLGM) in the southern Hengduan Mountain Range. It is located along the pathway which the ISM transports heat and moisture from the Bay of Bengal to inland China (Figures S1a and S1b in Supporting Information S1). The sediment proxy records from TCQH Lake well document the changes in the ISM intensity, vegetation and temperature since the LGP (Peng et al., 2019; Tian et al., 2019; X. Zhang et al., 2020; Zhao et al., 2021). Here we characterized EM variations over the LGP in Southwest China based on environmental magnetism proxies in two long sediment cores (TCQH4 and TCQH17A) from TCQH Lake (Figure S1c in Supporting Information S1). Accelerator mass spectrometry (AMS)  $^{14}\text{C}$  ages, combined with relative paleointensity (RPI) data indicated that the two cores contained material deposited continuously since approximately 90 kyr BP (before present, where present = 1950 A.D.; Z. Yang et al., 2022). Combined with the ISM intensity, which was previously reconstructed by the leaf wax hydrogen isotope ( $\delta\text{D}_{\text{wax}}$ ) record in the TCQH17A core (Zhao et al., 2021), we provide new insights into the terrestrial EM pattern in Southwest China since the LGP. Our data also provide evidence in support of the role of topography in modulating the Indo-Asian Monsoon circulation.

## 2. Materials and Methods

### 2.1. Materials and Sampling

TCQH Lake is a closed volcanic dammed lake without input from external rivers. The terrigenous debris of the lake sediments are mainly derived from the surrounding hills. The relatively detailed geological and geographical background of TCQH Lake and the sediment properties of two cores have been described by Peng et al. (2019) and X. Zang et al. (2022). A total of 679 and 1,068 discrete sediment samples were taken at  $\sim 2.5$  and  $\sim 2$  cm stratigraphic intervals from the TCQH4 and TCQH17A cores, respectively. We performed diffuse reflectance spectroscopy (DRS) and out of phase susceptibility ( $\chi_{\text{op}}$ ) on the samples from the TCQH17A core, and grain size analysis on all samples from the TCQH4 core. We also conducted DRS on 16 modern surface soil samples ( $\sim 10$  cm under the surface), sampled from the western foothill of GLGM at  $\sim 50$  m altitude interval from 2,250 to 3,050 m in 2019 A.D. (Figure S2 and Table S1 in Supporting Information S1).

### 2.2. Experimental Methods

The DRS measurements were conducted to obtain the relative concentration of hematite and goethite. The DRS was conducted on a PerkinElmer Lambda 950 spectrophotometer with a diffuse reflectance attachment (reflectance sphere) following analytical protocols described in T. Zhang et al. (2020). The data processing process was conducted following Scheinost (1998) and Torrent & Barrón. (2008). The out-of-phase susceptibility was measured for the TCQH17A samples using a Kappabridge KLY-5 with a frequency of 1220 Hz (which similar with  $\chi_{\text{fd}}$ ; Hrouda et al., 2013). Grain size components was measured for all TCQH4 samples using a Mastersizer 3,000 laser diffraction particle size analyzer.

### 2.3. Data Analytical Methods

The relative concentrations of hematite ( $\text{Rel}_{\text{Hm}}$ ), goethite ( $\text{Rel}_{\text{Gt}}$ ) and nanometer-scale ferrimagnetic minerals ( $\text{Rel}_{\chi_{\text{op}}}$ ) were calculated as follows:

$$\text{Rel}_{p_i} = n * \left( \frac{V_{p_i}}{\sum_{i=1}^n V_{p_i}} \right) \quad (1)$$

where  $V_p$  indicates the proxy value and  $n$  denotes the number of samples (Q. Zhang et al., 2018). The ratio of  $\frac{\text{Rel}_{\text{Hm}}}{\text{Rel}_{(\text{Hm}+\text{Gt})}}$  and  $\frac{\text{Rel}_{\chi_{\text{op}}}}{\text{Rel}_{\text{Hm}}}$ , abbreviated as H/(H + G) and OP/H, respectively, were also calculated as hydroclimate proxies for this study. Data were smoothed using the bootstrap method with 1 kyr windows, and decomposed

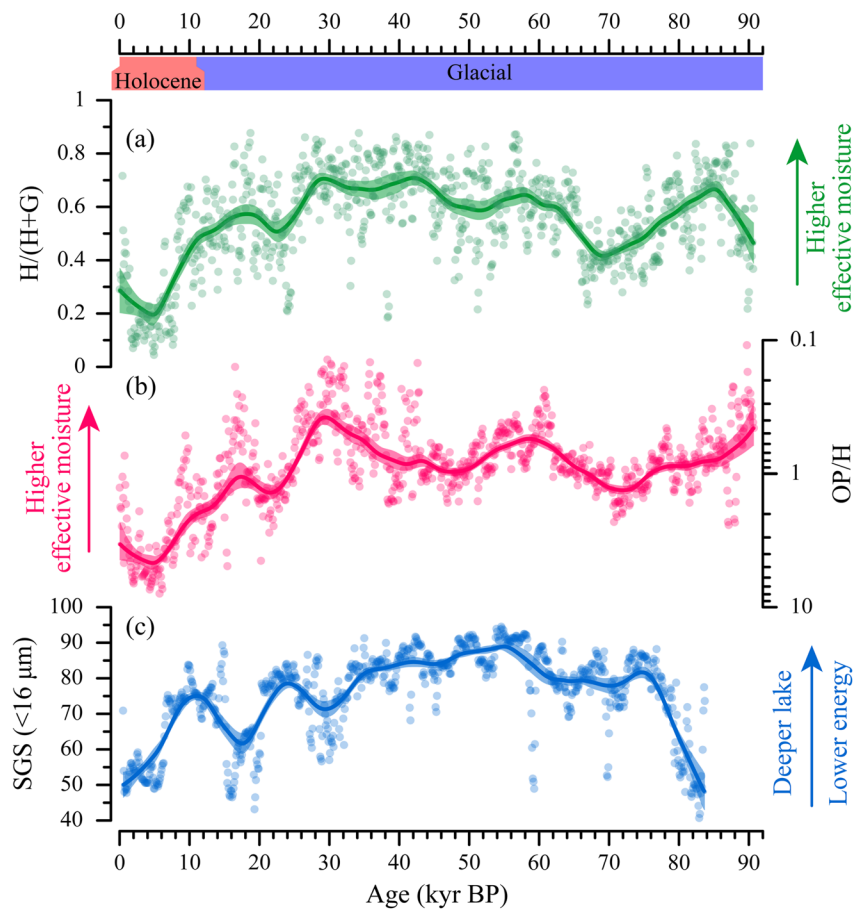


**Figure 1.** Proxy records from the two cores. (a)  $H/(H + G)$  record of TCQH17A; (b)  $OP/H$  record of TCQH17A; (c) small grain-size fraction record of TCQH4. Color dots represent the raw proxy data, thick solid lines represent smoothed data, and the shaded areas indicate 2-sigma confidence intervals.

using the ensemble empirical mode decomposition (EEMD) method in Acycle v2.3.1 (M. Li et al., 2019; Wu & Huang, 2009). Full details of the above experimental procedures and the data processing methods are provided in the Supporting Information S1 (Text S1).

### 3. Results

Modern climatic and observational data show that the annual mean temperature decreases with increasing elevation on the west slope of GLGM (Table S1 in Supporting Information S1; Xue, 1995), and the potential evapotranspiration also decreases with elevation according to the adjusted Thornthwaite method (1948). Annual mean precipitation and EM (precipitation minus evapotranspiration) increases with increasing elevation, and the maximum precipitation and EM occurs at the summit. Our elevation profile results for the surface soil show a linear positive correlation between  $H/(H + G)$  and EM (Figure S3 in Supporting Information S1), and  $OP/H$  is linearly negative with EM on a logarithmic scale (Figure S3 in Supporting Information S1).

Downcore variations of  $H/(H + G)$  and  $OP/H$  record from TCQH17A core and the small grain-size fraction (SGS,  $<16 \mu\text{m}$ ) record from TCQH4 core are shown in Figure 1. There is a strong similarity in variations of  $H/(H + G)$  and  $OP/H$  records at the orbital and sub-orbital scales, where the value of  $H/(H + G)$  show a decreasing trend during the periods of 90–70 and 30 kyr BP to the present, and an increasing trend from 70 to 30 kyr BP. It should be noted that the vertical axis of  $OP/H$  is inverted. The range of  $H/(H + G)$  is between 0.044 and 0.877, with a higher mean value of 0.591 during the LGP and 0.294 during the Holocene. The range of  $OP/H$  is between 0.109 and 7.904, with a lower mean value of 0.880 during the LGP and a higher mean value of 3.530 during the Holocene. Combined with the relationship between  $H/(H + G)$  and  $OP/H$  and EM from surface soil, we inferred

that the EM in the study area was higher during the LGP than during the Holocene. The SGS content of TCQH4 core range between 40% and 95%, with an average of 75% (Figure 1c). The SGS record is stable or showing slight change during the period of 70–30 kyr BP, with large fluctuations and a long-term decreasing trend during 30 kyr BP to the present. Overall, the three records reveal similar trends on the orbital scale and all show distinctly different characteristics during the glacial and interglacial stage, even though the SGS record differs from the other records at the millennial scale.

## 4. Discussion

### 4.1. Paleo-Effective Moisture Reconstruction Based on H/(H + G) and OP/H Proxies

Hematite, goethite and fine nanometer-scale ferrimagnetic minerals are common in soil and the formation of these minerals is largely controlled by surface environmental conditions (e.g., temperature, humidity; Jiang et al., 2022). Moreover, these minerals are formed competitively under different climatic conditions. Thus, H/(H + G) and the ratio of fine nanometer-scale ferrimagnets and hematite, which is often illustrated by frequency-dependent magnetic susceptibility/hard isothermal remanent magnetization ( $\chi_{fd}/\text{HIRM}$ ), are widely used for paleoprecipitation reconstruction (Ao et al., 2020; Hyland et al., 2015; Long et al., 2011; Nie et al., 2017). However, the relationship between the two ratios and precipitation is not immutable, and as precipitation increases, the interpretation of the ratios may be reversed due to mineral dissolution (Abrajevitch & Kodama, 2011; Z. Liu et al., 2013; Long et al., 2011). Annual mean precipitation of Tengchong (TC) and GLGM are higher than the threshold of 1,000 mm/yr, observed in previous study (Z. Liu et al., 2013). The relative concentration of goethite ( $\text{Rel}_{Gt}$ ), and ferrimagnetic minerals ( $\text{Rel}_{\chi_{op}}$ ) of surface soil samples shows a linearly anti-correlation with precipitation, which indicate the existence of mineral dissolution and the degree of dissolution was correlated with precipitation (Figure S3 in Supporting Information S1). In addition, Figures 3a–3c shows that hematite is more stable than goethite and ferrimagnetic minerals under dissolution environment (Abrajevitch & Kodama, 2011). Therefore, higher precipitation will theoretically lead to higher H/(H + G) and lower  $\chi_{fd}/\text{HIRM}$ , which is also supported by the result of surface soil from GLGM (Figure S3 in Supporting Information S1). It is important to note that very fine hematite does not carry a remanence signal, which may lead to an underestimation of the concentration of hematite using HIRM. Thus, we used  $\text{Rel}_{Hm}$  instead of HIRM to improve the accuracy of hematite content estimation. Since terrestrial moisture is not determined solely by precipitation, EM is more suitable to description of the hydroclimatic environment (wetter or drier) of a region than precipitation (S. Liu et al., 2018). EM is positively correlated with precipitation, so the correlation between EM, precipitation and two ratios (H/(H + G), OP/H) is similar (Figures S3j–S3k in Supporting Information S1). Additionally, the highly similar trends of H/(H + G) and OP/H in TCQH17A core also imply that two ratios are controlled by the same factors. The SGS record from TCQH4 shows a consistent trend with the SGS, Ti and black carbon records from TCQH10-1, taken from the same lake during the overlapping periods (Figure S4 in Supporting Information S1; E. L. Zhang et al., 2017). This also suggests that the variations of SGS content in the TCQH4 sediments may relate to lake level or EM changes (E. L. Zhang et al., 2017).

We next applied the EEMD method to analyze our H/(H + G) and OP/H records. The EEMD results show that the intrinsic mode functions (IMF) 1–5 of the two records mainly reflect climate variability at the centennial–millennial scale (Figure S5 in Supporting Information S1). The precession scale variability is captured by the IMF 6–7 of H/(H + G) and IMF6 of OP/H (Figure S5 in Supporting Information S1), which coincides with the simulated precipitation rate of South Asia (Kutzbach et al., 2008), the precession, and Northern Hemisphere summer insolation (NHSI; Figure S6 in Supporting Information S1; Laskar et al., 2004). This also supports the idea that orbital-scale variability of ISM is driven by precession induced changes in NHSI which is based on numerous studies from marine and terrestrial proxies (Bolton et al., 2013; Cai et al., 2015; Dutt et al., 2015; Kathayat et al., 2016; Mohtadi et al., 2016). In general, minimum precession is reached when the Northern Hemisphere summer solstice occurs at perihelion, which results in the higher insolation and stronger land–sea thermal gradient in the Northern Hemisphere (Mohtadi et al., 2016). Higher insolation increases the temperature, evapotranspiration and atmospheric humidity. The stronger thermal gradient enhances the atmosphere circulation and wind speed (enhances the ISM), which transports more moisture from ocean to land, increasing precipitation in the monsoonal region. The wetness brought by increase precipitation counteracts the dryness induced by increase evapotranspiration, resulting in the increased of EM and a wetter climate. The majority of the moisture from TC is transported from the Bay of Bengal and Indian Ocean via the ISM during the monsoon season (An et al., 2011;

Cai et al., 2015; Y. Yang et al., 2019). The major finding from our records is that the minimum of our  $H/(H + G)$  correlates well with the maximum of precession and the minimum of simulate precipitation and insolation, and vice versa (Figure S6 in Supporting Information S1; Kutzbach et al., 2008; Laskar et al., 2004). However, the opposite is observed for  $OP/H$ , which is consistent with the results from GLGM surface soils. Therefore,  $H/(H + G)$  and  $OP/H$  were considered to be reliable proxies for paleo-EM reconstruction in this study.

We stacked  $H/(H + G)$  and  $OP/H$  records into a new synthesized curve after standardization to characterize the variation of EM in the TC region since 90 kyr BP (Figure S7 in Supporting Information S1). The stacked curve suggests that the EM decreased continuously during 90–70 kyr BP. Subsequently, EM increased slowly with fluctuation from 70 to 30 kyr BP and reached the maximum at ~30 kyr BP. EM then decreased rapidly during 30–22 kyr BP, and continued to decrease after a brief increase at 22–18 kyr BP, reaching its minimum at ~4 kyr BP, which is consistent with the lower lake level reconstructed by SGS and Ti concentration (Figure S4 in Supporting Information S1; E. L. Zhang et al., 2017). Subsequently, the EM increased from 4 kyr BP to the present.

#### 4.2. Decoupling of Effective Moisture and ISM Modulated by Temperature and Topography

The most profound feature of our stacked curve is that the hydroclimate of TC during glacial stages is wetter (higher EM) than the interglacial stages, which is also supported by our grain size results (higher SGS contents). This wetter glacial pattern is opposite to the general consensus of a weakened monsoon and reduced monsoon rainfall during glacial stages (Cai et al., 2015; X. Zhang et al., 2020; Zhao et al., 2021). A similar wetter glacial pattern has also been observed in other continental records from easternmost Africa (Dinezio & Tierney, 2013), southwestern United States (Railsback et al., 2015) and southeastern rim of the Alps (Spötl et al., 2021). They suggested that the increased more rainfall in the regions mentioned above during the glacial stages may be explained by changes in the intensity and location of atmosphere convection, resulting in changes in the moisture transport pathway and amount of water vapor. However, the trajectory of moisture advection from the Bay of Bengal to the TC region is relatively stable during the present day and the Last Glacial Maximum (LGM; Cai et al., 2015). Weakened ISM during glacial stage was also observed in the  $\delta D_{\text{wax}}$  record from the TCQH17A core (Zhao et al., 2021), terrestrial stalagmite  $\delta^{18}\text{O}$  records (Cai et al., 2015; Dutt et al., 2015; Kathayat et al., 2016) and ocean sediments derived ISM records (Caley et al., 2011; Clemens & Prell, 2003; Lauterbach et al., 2020) from different locations in the ISM domain (Figure 2). There should be less moisture transport and precipitation in TC given the weakened ISM and lower temperatures and weakened convection during the glacial stage, which is opposite to the increased EM observed in our record. This seems to indicate that not only the temperature and ISM are decoupled at the orbital scale in TC (Zhao et al., 2021), but EM and monsoon are also decoupled.

EM is controlled by precipitation and evapotranspiration, the latter being closely related to temperature. Empirical studies have shown that temperature rise markedly affects the severity of droughts, and the evaporation and transpiration can consume up to 80% of precipitation based on a general circulation model experiment (Abramopoulos et al., 1988; Vicente-Serrano et al., 2010). In addition, the dryness brought by increased temperature is comparable to that induced by decreased precipitation (Abramopoulos et al., 1988). Conversely, the wetness brought by decreased temperature (evapotranspiration) can counteract the dryness induced by decreased precipitation (S. Liu et al., 2018). Modern meteorological data show that the long-term mean annual precipitation (1,495 mm) is comparable to evapotranspiration (1,591 mm) in TC. Therefore, precipitation and temperature anomalies can have a non-negligible impact on EM in TC. Temperature records reconstructed from multiple proxies show that glacial temperatures in TC were lower than interglacial (Figure S8 in Supporting Information S1). The sustained increase in temperature since 20 kyr BP has led to a continuous increase in evapotranspiration, which may have led to a decrease in EM, even though the monsoon was enhanced during the interglacial phase. This results in decoupling pattern of EM and ISM.

Modern meteorological data show that the distribution of ISM EM and precipitation are concentrated in three regions: the southern side of the Himalayas; the west coast of the continent and some inland areas (Figure 3a; Figure S9 in Supporting Information S1). A common feature of these areas is that they are all located on the windward side of mountains during the ISM season. The precipitation distribution pattern has an excellent relationship with topography, which is also consistent with the view that topography can modify precipitation patterns by redistributing airflow (Acosta & Huber, 2020; Thomson et al., 2021; Xie et al., 2006). Theoretically, owing to the land-sea thermal gradient in summer, ISM wind carries a large amount of water vapor from ocean to land. The



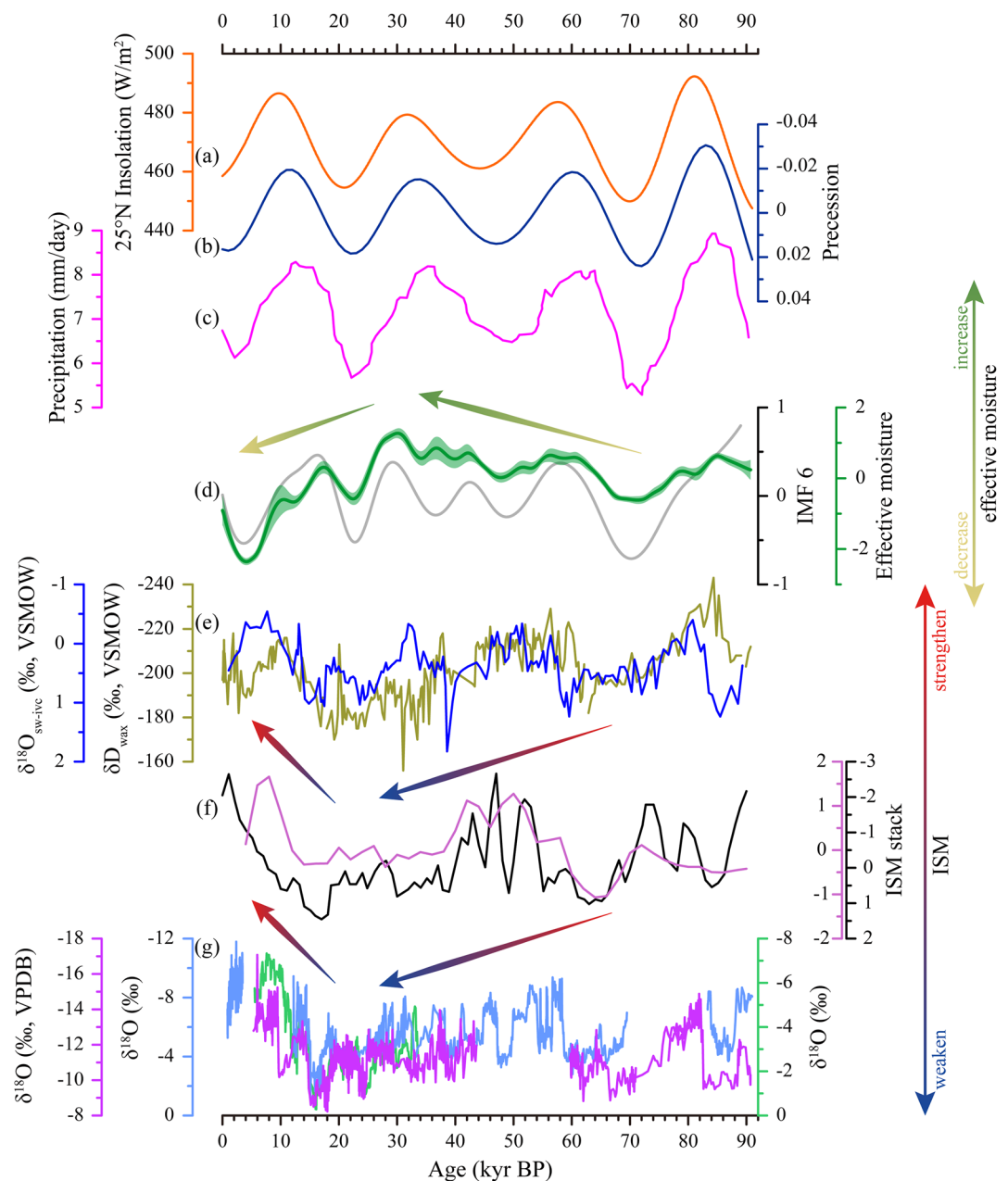


**Figure 2.** Comparison of the reconstructed effective moisture (EM) record from Tenchong Qinghai Lake and related records. (a) Northern Hemisphere summer insolation (25°N, June–August; Laskar et al., 2004); (b) precession (Laskar et al., 2004); (c) simulated precipitation of south Asia region (Kutzbach et al., 2008); (d) stacked EM record of the TCQH17A core (grass green line) and EEMD-IMF 6 record (gray line); (e)  $\delta D_{wax}$  record of the TCQH17A core (Zhao et al., 2021) and  $\delta^{18}O_{sw-ivc}$  record of SO 188-17286-1 core (Lauterbach et al., 2020); (f) Indian summer monsoon stack records (Caley et al., 2011; Clemens & Prell, 2003); (g) stalagmite  $\delta^{18}O$  records from Xiaobailong Cave (Cai et al., 2015), Bittoo cave (Kathayat et al., 2016), and Mawmluh cave (Dutt et al., 2015).

warm and moist atmospheric flow will uplift along the windward slope after encountering the mountain, and the water vapor cools, condenses, grows and then falls as raindrops as it rises over a mountain. The remaining water vapor continues to migrate to the destination. For meso-minor scale mountains, there is more rainfall on the windward slope and the maximum is observed near the summit (Figure 3b; Ramage & Schroeder, 1999). In contrast, it is more difficult for water vapor to climb over large-scale mountains, which cause higher (lower) precipitation at lower (higher) altitudes (Figure 3b). In addition, the temperature and evapotranspiration are influenced by large-scale topography (Figure S9 in Supporting Information S1).

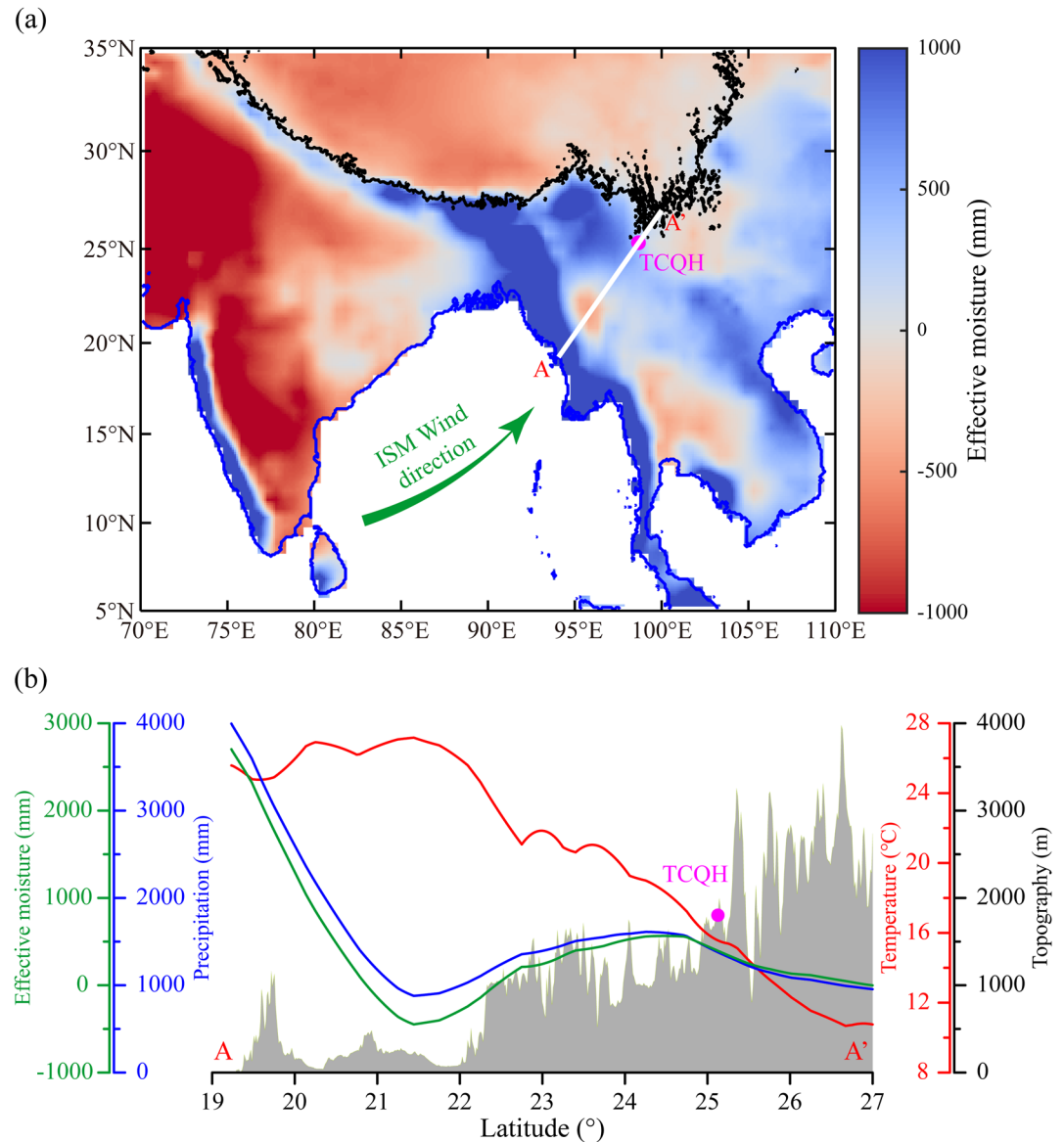


**Figure 3.** Modern climatology of the study sites. (a) Long-term mean annual effective moisture (EM) distributions during 1961–2010, blue lines indicate the present coastline, the black lines denote the boundary of topography at 3,000 m above sea level; (b) profiles of topography (gray shading), annual temperature (red line), annual precipitation (blue line) and annual EM (green line) from A to A' in (a). The location of Tenchong Qinghai Lake is indicated by a magenta dot.

It is worth noting that TC is located on the southwestern windward side of the Hengduan Mountains. The monsoon precipitation in TC is higher than that in inland areas because of the topographic uplift effect of the Hengduan mountains and the Yunnan-Guizhou Plateau, which act as a dynamic barrier to monsoon wind and water vapor. The special geographical location and topography imply that the terrain factors may be responsible for the decoupling of EM and monsoon in TC.

During the glacial stage, the water vapor is transported at a lower-level because of to the relative cold continent. It is difficult for water vapor to climb over the Hengduan mountains under weakened ISM and lower transport energy (lower wind speed), leading to the accumulation of precipitation on the windward slope of the mountains and shortage of precipitation in inland. The model simulation results also show that the precipitation in TC during the LGM was comparable or even slightly higher than present (Figure S10 in Supporting Information S1). In addition, the evapotranspiration is decreased by the intense cooling during the glacial stage, resulting in increased EM in TC (Figure 4a). In contrast, in the interglacial stage with enhanced ISM, the warmer land alters the surface

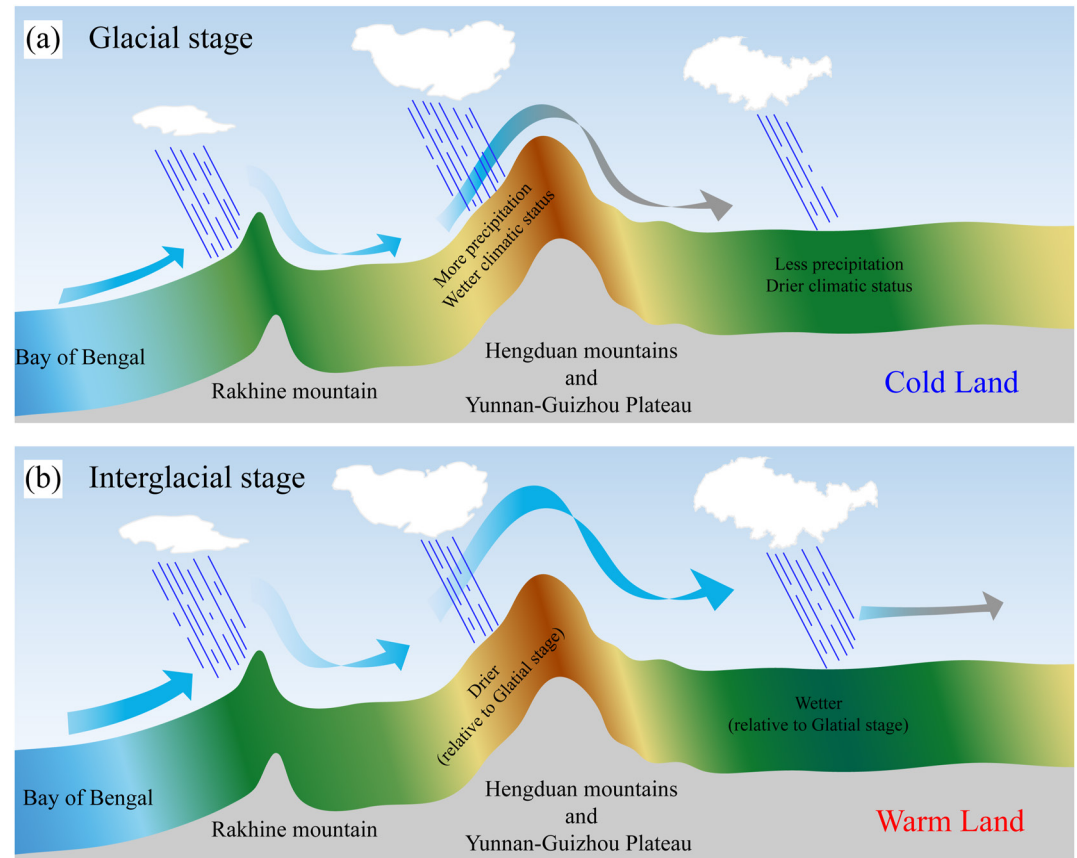


**Figure 4.** Schematic diagram illustrating the decoupling pattern between Indian summer monsoon and precipitation influenced by temperature and topography during different climatic status. (a) Glacial stage; (b) interglacial stage.

temperature structure, and water vapor is transported at a relatively higher level under the thermal uplifting forces the land. The water vapor can more easily climb over the mountains and is transported inland under a higher transport energy (higher wind speed) and lower lifting energy, bringing more precipitation to inland (Figure 4b). However, the dryness from increased evaporation due to warming outweighs the wetness from an enhanced monsoon and increased precipitation, resulting in decreased EM in TC (Figure 4b). Eventually, the EM in the TC is decoupled with the ISM intensity at the glacial-interglacial scale under the combined influence of temperature and topography.

## 5. Conclusions

We present the high-resolution EM records in Southwestern China spanning the last glacial stage based on  $H/(H + G)$  and  $OP/H$ . Our results show that the variability of EM at the orbital scale in the TC region is primarily dominated by precession, and TC experienced a profound humid and relatively arid hydroclimate during the glacial and interglacial stage, respectively. These findings demonstrate that the EM was decoupled with ISM in this region during the last glacial-interglacial cycle. The modern meteorological data suggest that temperature and topography may play an indispensable role in regulating the hydroclimate and the decoupled relationship between monsoon and EM in Southwestern China. This research indicates a strong effect of temperature and topography on climate over long time scales. However, further detailed investigations in other regions and proxies are needed to improve global climate models and provide more accurate simulations of the Earth's past, present, and future climate states.



## Conflict of Interest

The authors declare no conflicts of interest relevant to this study.

## Data Availability Statement

The raw data used in this study is accessible from the Pangaea data repository (<https://doi.org/10.1594/PANGAEA.958273>). The meteorological data are obtained from CRU TS v4.06 datasets (Harris et al., 2020) and CHLSA-TraCE21k datasets (Karger et al., 2017).

## Acknowledgments

The authors thank two anonymous reviewers for their helpful and constructive reviews of the manuscript, and thank LetPub ([www.letpub.com](http://www.letpub.com)) for linguistic assistance and pre-submission expert review. This research is supported by the projects of National Second Expedition to the Tibetan Plateau (2019QZKK0707), Guangdong Province Introduced Innovative R&D Team of Geological Processes and Natural Disasters around the South China Sea (2016ZT06N331), the projects of National Natural Science Foundation of China (41872217, 41672162, 41904068).

## References

- Abrajewitch, A., & Kodama, K. (2011). Diagenetic sensitivity of paleoenvironmental proxies: A rock magnetic study of Australian continental margin sediments. *Geochemistry, Geophysics, Geosystems*, 12(5), Q05Z24. <https://doi.org/10.1029/2010gc003481>
- Abramopoulos, F., Rosenzweig, C., & Choudhury, B. (1988). Improved ground hydrology calculations for global climate models (GCMs): Soil water movement and evapotranspiration. *Journal of Climate*, 1(9), 921–941. [https://doi.org/10.1175/1520-0442\(1988\)001<0921:lgchfg>2.0.Co;2](https://doi.org/10.1175/1520-0442(1988)001<0921:lgchfg>2.0.Co;2)
- Acosta, R. P., & Huber, M. (2020). Competing topographic mechanisms for the summer Indo-Asian monsoon. *Geophysical Research Letters*, 47(3), e2019GL085112. <https://doi.org/10.1029/2019GL085112>
- An, Z., Clemens, S. C., Shen, J., Qiang, X., Jin, Z., Sun, Y., et al. (2011). Glacial-interglacial Indian summer monsoon dynamics. *Science*, 333(6043), 719–723. <https://doi.org/10.1126/science.1203752>
- Ao, H., Rohling, E. J., Stringer, C., Roberts, A. P., Dekkers, M. J., Dupont-Nivet, G., et al. (2020). Two-stage mid-Brunhes climate transition and mid-Pleistocene human diversification. *Earth-Science Reviews*, 210, 103354. <https://doi.org/10.1016/j.earscirev.2020.103354>
- Bolton, C. T., Chang, L., Clemens, S. C., Kodama, K., Ikehara, M., Medina-Elizalde, M., et al. (2013). A 500,000 year record of Indian summer monsoon dynamics recorded by eastern equatorial Indian Ocean upper water-column structure. *Quaternary Science Reviews*, 77, 167–180. <https://doi.org/10.1016/j.quascirev.2013.07.031>
- Cai, Y., Fung Inez, Y., Edwards, R. L., An, Z., Cheng, H., Lee, J.-E., et al. (2015). Variability of stalagmite-inferred Indian monsoon precipitation over the past 252,000 y. *Proceedings of the National Academy of Sciences*, 112(10), 2954–2959. <https://doi.org/10.1073/pnas.1424035112>
- Caley, T., Malaizé, B., Zaragosi, S., Rossignol, L., Bourget, J., Eynaud, F., et al. (2011). New Arabian Sea records help decipher orbital timing of Indo-Asian monsoon. *Earth and Planetary Science Letters*, 308(3), 433–444. <https://doi.org/10.1016/j.epsl.2011.06.019>
- Cheng, H., Edwards, R. L., Sinha, A., Spötl, C., Yi, L., Chen, S., et al. (2016). The Asian monsoon over the past 640,000 years and ice age terminations. *Nature*, 534(7609), 640–646. <https://doi.org/10.1038/nature18591>
- Clemens, S. C., & Prell, W. L. (2003). A 350,000 year summer-monsoon multi-proxy stack from the Owen Ridge, Northern Arabian Sea. *Marine Geology*, 201(1), 35–51. [https://doi.org/10.1016/S0025-3227\(03\)00207-X](https://doi.org/10.1016/S0025-3227(03)00207-X)
- Dinezio, P. N., & Tierney, J. E. (2013). The effect of sea level on glacial Indo-Pacific climate. *Nature Geoscience*, 6(6), 485–491. <https://doi.org/10.1038/ngeo1823>
- Ding, Y., Liang, P., Liu, Y., & Zhang, Y. (2020). Multiscale variability of Meiyu and its prediction: A new review. *Journal of Geophysical Research: Atmospheres*, 125(7), e2019JD031496. <https://doi.org/10.1029/2019JD031496>
- Dutt, S., Gupta, A. K., Clemens, S. C., Cheng, H., Singh, R. K., Kathayat, G., & Edwards, R. L. (2015). Abrupt changes in Indian summer monsoon strength during 33,800 to 5500 years B.P. *Geophysical Research Letters*, 42(13), 5526–5532. <https://doi.org/10.1002/2015GL064015>
- Harris, I., Osborn, T. J., Jones, P., & Lister, D. (2020). Version 4 of the CRU TS monthly high-resolution gridded multivariate climate dataset. *Scientific Data*, 7(1), 109. <https://doi.org/10.1038/s41597-020-0453-3>
- Hrouda, F., Pokorný, J., Ježek, J., & Chadima, M. (2013). Out-of-phase magnetic susceptibility of rocks and soils: A rapid tool for magnetic granulometry. *Geophysical Journal International*, 194(1), 170–181. <https://doi.org/10.1093/gji/ggt097>
- Hyland, E. G., Sheldon, N. D., Van der Voo, R., Badgley, C., & Abrajewitch, A. (2015). A new paleoprecipitation proxy based on soil magnetic properties: Implications for expanding paleoclimate reconstructions. *Bulletin*, 127(7–8), 975–981. <https://doi.org/10.1130/B31207.1>
- Jiang, Z., Liu, Q., Roberts, A. P., Dekkers, M. J., Barrón, V., Torrent, J., & Li, S. (2022). The magnetic and color reflectance properties of hematite: From Earth to Mars. *Reviews of Geophysics*, 60(1), e2020RG000698. <https://doi.org/10.1029/2020RG000698>
- Jin, Q., & Wang, C. (2017). A revival of Indian summer monsoon rainfall since 2002. *Nature Climate Change*, 7(8), 587–594. <https://doi.org/10.1038/nclimate3348>
- Karger, D. N., Conrad, O., Böhrer, J., Kawohl, T., Kreft, H., Soria-Auza, R. W., et al. (2017). Climatologies at high resolution for the Earth's land surface areas. *Scientific Data*, 4(1), 170122. <https://doi.org/10.1038/sdata.2017.122>
- Kathayat, G., Cheng, H., Sinha, A., Spötl, C., Edwards, R. L., Zhang, H., et al. (2016). Indian monsoon variability on millennial-orbital timescales. *Scientific Reports*, 6(1), 24374. <https://doi.org/10.1038/srep24374>
- Kathayat, G., Sinha, A., Breitenbach, S. F. M., Tan, L., Spötl, C., Li, H., et al. (2022). Protracted Indian monsoon droughts of the past millennium and their societal impacts. *Proceedings of the National Academy of Sciences of the United States of America*, 119(39), e2207487119. <https://doi.org/10.1073/pnas.2207487119>
- Kutzbach, J. E., Liu, X., Liu, Z., & Chen, G. (2008). Simulation of the evolutionary response of global summer monsoons to orbital forcing over the past 280,000 years. *Climate Dynamics*, 30(6), 567–579. <https://doi.org/10.1007/s00382-007-0308-z>
- Laskar, J., Robutel, P., Joutel, F., Gastineau, M., Correia, A. C. M., & Levrard, B. (2004). A long-term numerical solution for the insolation quantities of the Earth. *Astronomy and Astrophysics*, 428(1), 261–285. <https://doi.org/10.1051/0004-6361:20041335>
- Lauterbach, S., Andersen, N., Wang, Y. V., Blanz, T., Larsen, T., & Schneider, R. R. (2020). An ~130 kyr record of surface water temperature and  $\delta^{18}\text{O}$  from the northern Bay of Bengal: Investigating the linkage between Heinrich events and weak monsoon intervals in Asia. *Paleoceanography and Paleoclimatology*, 35(2), e2019PA003646. <https://doi.org/10.1029/2019PA003646>
- Li, M., Hinnov, L., & Kump, L. (2019). Acycle: Time-series analysis software for paleoclimate research and education. *Computers & Geosciences*, 127, 12–22. <https://doi.org/10.1016/j.cageo.2019.02.011>
- Li, S., Wang, T., Huang, X., Pu, X., Li, M., Chen, P., et al. (2018). Impact of East Asian summer monsoon on surface ozone pattern in China. *Journal of Geophysical Research: Atmospheres*, 123(2), 1401–1411. <https://doi.org/10.1002/2017JD027190>

- Li, X., & Tang, Y. (2021). Predictable pattern of precipitation over Asian summer monsoon regions. *Geophysical Research Letters*, 48(22), e2021GL095824. <https://doi.org/10.1029/2021GL095824>
- Liu, S., Jiang, D., & Lang, X. (2018). A multi-model analysis of moisture changes during the last glacial maximum. *Quaternary Science Reviews*, 191, 363–377. <https://doi.org/10.1016/j.quascirev.2018.05.029>
- Liu, Z., Liu, Q., Torrent, J., Barrón, V., & Hu, P. (2013). Testing the magnetic proxy  $\chi_{FD}/HIRM$  for quantifying paleoprecipitation in modern soil profiles from Shaanxi Province, China. *Global and Planetary Change*, 110, 368–378. <https://doi.org/10.1016/j.gloplacha.2013.04.013>
- Long, X., Ji, J., & Balsam, W. (2011). Rainfall-dependent transformations of iron oxides in a tropical saprolite transect of Hainan Island, South China: Spectral and magnetic measurements. *Journal of Geophysical Research*, 116(F3), F03015. <https://doi.org/10.1029/2010JF001712>
- Man, W., Zhou, T., & Jungclauss, J. H. (2014). Effects of large volcanic eruptions on global summer climate and East Asian monsoon changes during the last millennium: Analysis of MPI-ESM simulations. *Journal of Climate*, 27(19), 7394–7409. <https://doi.org/10.1175/JCLI-D-13-00739.1>
- Mohtadi, M., Prange, M., & Steinke, S. (2016). Palaeoclimatic insights into forcing and response of monsoon rainfall. *Nature*, 533(7602), 191–199. <https://doi.org/10.1038/nature17450>
- Nie, J., Garziona, C., Su, Q., Liu, Q., Zhang, R., Heslop, D., et al. (2017). Dominant 100,000-year precipitation cyclicity in a late Miocene lake from northeast Tibet. *Science Advances*, 3(3), e1600762. <https://doi.org/10.1126/sciadv.1600762>
- Peng, J., Yang, X. Q., Toney, J. L., Ruan, J. Y., Li, G. H., Zhou, Q. X., et al. (2019). Indian Summer Monsoon variations and competing influences between hemispheres since ~35 ka recorded in Tengchongqinghai Lake, southwestern China. *Palaeogeography, Palaeoclimatology, Palaeoecology*, 516, 113–125. <https://doi.org/10.1016/j.palaeo.2018.11.040>
- Railsback, L. B., Brook, G. A., Ellwood, B. B., Liang, F., Cheng, H., & Edwards, R. L. (2015). A record of wet glacial stages and dry interglacial stages over the last 560 kyr from a standing massive stalagmite in Carlsbad Cavern, New Mexico, USA. *Palaeogeography, Palaeoclimatology, Palaeoecology*, 438, 256–266. <https://doi.org/10.1016/j.palaeo.2015.08.010>
- Ramage, C. S., & Schroeder, T. A. (1999). Trade wind rainfall atop Mount Waialeale, Kauai. *Monthly Weather Review*, 127(9), 2217–2226. [https://doi.org/10.1175/1520-0493\(1999\)127<2217:TWRAMW>2.0.CO;2](https://doi.org/10.1175/1520-0493(1999)127<2217:TWRAMW>2.0.CO;2)
- Scheinost, A. C. (1998). Use and limitations of second-derivative diffuse reflectance spectroscopy in the visible to near-infrared range to identify and quantify Fe oxide minerals in soils. *Clays and Clay Minerals*, 46(5), 528–536. <https://doi.org/10.1346/CCMN.1998.0460506>
- Spötl, C., Koltai, G., Jarosch, A. H., & Cheng, H. (2021). Increased autumn and winter precipitation during the Last Glacial Maximum in the European Alps. *Nature Communications*, 12(1), 1–9. <https://doi.org/10.1038/s41467-021-22090-7>
- Thomson, J. R., Holden, P. B., Anand, P., Edwards, N. R., Porchier, C. A., & Harris, N. B. W. (2021). Tectonic and climatic drivers of Asian monsoon evolution. *Nature Communications*, 12(1), 1–10. <https://doi.org/10.1038/s41467-021-24244-z>
- Thorntwaite, C. W. (1948). An approach toward a rational classification of climate. *Geographical Review*, 38(1), 55–94. <https://doi.org/10.2307/210739>
- Tian, L. P., Wang, M. Y., Zhang, X., Yang, X. Q., Zong, Y. Q., Jia, G. D., et al. (2019). Synchronous change of temperature and moisture over the past 50 ka in subtropical southwest China as indicated by biomarker records in a crater lake. *Quaternary Science Reviews*, 212, 121–134. <https://doi.org/10.1016/j.quascirev.2019.04.003>
- Torrent, J., & Barrón, V. (2008). Diffuse reflectance spectroscopy. In J. Torrent & V. Barrón (Eds.), *Methods of soil analysis Part 5—Mineralogical methods* (pp. 367–385). Soil Science Society of America. <https://doi.org/10.2136/sssabookser5.5.c13>
- Vicente-Serrano, S. M., Beguería, S., & López-Moreno, J. I. (2010). A multiscalar drought index sensitive to global warming: The standardized precipitation evapotranspiration index. *Journal of Climate*, 23(7), 1696–1718. <https://doi.org/10.1175/2009jcli2909.1>
- Wu, Z., & Huang, N. E. (2009). Ensemble empirical mode decomposition: A noise-assisted data analysis method. *Advances in Adaptive Data Analysis*, 01(01), 1–41. <https://doi.org/10.1142/S1793536909000047>
- Xie, S. P., Xu, H., Saji, N. H., Wang, Y., & Liu, W. T. (2006). Role of narrow mountains in large-scale organization of Asian monsoon convection. *Journal of Climate*, 19(14), 3420–3429. <https://doi.org/10.1175/JCLI3777.1>
- Xue, J. R. (Ed.). (1995). *Gaoligong mountain national nature reserve*. Chinese Forestry Publishing House.
- Yang, X., Zhang, T., Zhang, E., Toney, J., Zhou, Q., & Xie, Y. (2022). Paleosecular variations during the last glacial period from Tengchong Qinghai Lake, Yunnan Province, China. *Journal of Geophysical Research: Solid Earth*, 127(3), e2021JB023459. <https://doi.org/10.1029/2021JB023459>
- Yang, Y., Yang, R., Cao, J., Zhao, J., Cheng, H., & Wang, J. (2019). Relationship between the Asian summer monsoon circulation and speleothem  $\delta^{18}\text{O}$  of Xiaobailong cave. *Climate Dynamics*, 53(9–10), 6351–6362. <https://doi.org/10.1007/S00382-019-04935-6>
- Zhang, E. L., Zhao, C., Xue, B., Liu, Z. H., Yu, Z. C., Chen, R., & Shen, J. (2017). Millennial-scale hydroclimate variations in southwest China linked to tropical Indian Ocean since the Last Glacial Maximum. *Geology*, 45(5), 435–438. <https://doi.org/10.1130/G38309.1>
- Zhang, Q., Liu, Q., Li, J., & Sun, Y. (2018). An Integrated study of the eolian dust in pelagic sediments from the North Pacific Ocean based on environmental magnetism, transmission electron microscopy, and diffuse reflectance spectroscopy. *Journal of Geophysical Research: Solid Earth*, 123(5), 3358–3376. <https://doi.org/10.1002/2017jb014951>
- Zhang, R., Jiang, D., Zhang, Z., & Yu, E. (2015). The impact of regional uplift of the Tibetan Plateau on the Asian monsoon climate. *Palaeogeography, Palaeoclimatology, Palaeoecology*, 417, 137–150. <https://doi.org/10.1016/j.palaeo.2014.10.030>
- Zhang, T., Yang, X., Chen, Q., Toney, J. L., Zhou, Q., & Gao, H. (2020). Humidity variations spanning the ‘Little Ice Age’ from an upland lake in southwestern China. *The Holocene*, 30(2), 289–299. <https://doi.org/10.1177/0959683619883026>
- Zhang, X., Zheng, Z., Huang, K., Yang, X., & Tian, L. (2020). Sensitivity of altitudinal vegetation in southwest China to changes in the Indian summer monsoon during the past 68000 years. *Quaternary Science Reviews*, 239, 106359. <https://doi.org/10.1016/j.quascirev.2020.106359>
- Zhao, C., Rohling, E. J., Liu, Z., Yang, X., Zhang, E., Cheng, J., et al. (2021). Possible obliquity-forced warmth in southern Asia during the last glacial stage. *Science Bulletin*, 66(11), 1136–1145. <https://doi.org/10.1016/j.scib.2020.11.016>
- Zhou, X., Ding, Y., & Wang, P. (2010). Moisture transport in the Asian summer monsoon region and its relationship with summer precipitation in China. *Acta Meteorologica Sinica*, 24(1), 31–42. <http://jmr.cmsjournal.net/en/article/id/1231>